Multi-Objective Robust Optimization for a Dual-Flux-Modulator Coaxial Magnetic Gear

Liu, X.; Zhao, Y.; Chen, Z.; Luo, D.; Huang, S.

Published in:
IEEE Transactions on Magnetics

DOI (link to publication from Publisher):
10.1109/TMAG.2018.2887273

Publication date:
2019

Document Version
Accepted author manuscript, peer reviewed version

Multi-Objective Robust Optimization for a Dual-Flux-Modulator Coaxial Magnetic Gear

Xiao Liu[1], Yunyun Zhao[1], Zhe Chen[2], Derong Luo[1], and Shoudao Huang[1]

[1]College of Electrical and Information Engineering, Hunan University, Changsha 410082, China
[2]Department of Energy Technology, Aalborg University, 9220 Aalborg East, Denmark

The conventional multi-objective deterministic optimization (MODO) design may be less meaningful or even unacceptable when considering the perturbations of design parameters and reliability of the optimization results. In order to overcome the above-mentioned drawback and improve both the torque capability and permanent magnet (PM) utilization efficiency of dual-flux-modulator coaxial magnetic gear (DFM-CMG) simultaneously, a robust optimization design method is presented. In this method, the sigma criteria with the Monte Carlo simulation (MCS) are adopted to obtain the statistic samples addressing the effects of parametric uncertainties of DFM-CMG on the optimization results. Both 2-D and 3-D finite-element (FE) models of a DFM-CMG are first established, and the 3-D FE model is proven more accurate by the experiment and used for further optimization. Through the parametric study, five parameters are selected as the key design variables to establish the quadratic polynomial regression metamodels. Finally, the multi-objective particle swarm optimization algorithm with MCS is employed to conduct the multi-objective robust optimization (MORO) for DFM-CMG. Although the stall torque per PM consumption achieved by MORO with six sigma (6σ) is little lower than that achieved by MODO, it still has a 21.4% growth than that of the initial design under the same constraint of the stall torque. Furthermore, the reliability and stability of the MORO results are much higher than those of the MODO results. The MORO method is significantly effective as the torque performance and robustness of DFM-CMG could be improved simultaneously.

Index Terms— **Dual-flux-modulator coaxial magnetic gear (DFM-CMG), finite-element method (FEM), multi-objective robust optimization (MORO), reliability and stability, torque performance.**

I. Introduction

COAXIAL magnetic gears (CMGs) have drawn increasing attention because they could realize noncontact torque and speed transmission by the interaction of the modulated magnetic fields in the air gaps [1], [2]. These CMGs take the advantages of low friction loss, minimum acoustic noise, and no maintenance. A dual-flux-modulator coaxial magnetic gear (DFM-CMG), characterized a higher torque capability and higher permanent magnet (PM) utilization efficiency comparing to other CMGs, was proposed in [3]. Although the steady-state performance of DFM-CMG has been studied, the optimal design of DFM-CMG needs to be further investigated.

Deterministic optimization has been successfully applied for the designs of CMG to improve the torque capability. The multiple linear regression analysis based on the non-linear 2-D finite-element method (FEM) was used to improve the low torque density of a hybrid magnetic torque converter-based conventional CMG by optimizing the rotor shape [4]. The FEM-genetic algorithm-coupled method was applied to optimize the dimensions of a CMG PM machine with the aim of improving the torque performance [5]. The single objective deterministic optimal design method for a dual-mechanical port machine with the flux modulation effect was presented in [6]. The multi-objective deterministic optimization (MODO) has been applied to the conventional CMG to improve the torque capability [7]. Unfortunately, the deterministic optimization method may become less meaningful when considering the possible variation and uncertainty of design variables caused by manufacturing and assembling [8]. Moreover, the existence of fluctuation in design variables or operation conditions has a great influence on the CMG torque performance [9]. Therefore, the uncertainty of the design parameters must be considered for a robust optimal design.

Most existing robust designs for electromagnetic devices with PM only deal with the single objective optimization [10], [11]. However, with emphasis on the cost, the comparative result between CMGs with non-rare-earth and rare-earth PMs shows that the stall torque (ST) conflicts with the PM material consumption each other [12]. Therefore, it is very essential to maximize the torque performance including both the ST and ST per PM consumption (STPPC) and improve the robustness of DFM-CMG considering the uncertainties of design parameters simultaneously. To our knowledge, there is little attention to study the robust optimal design of CMG. Resultantly, studies on the multi-objective robust optimization (MORO) for DFM-CMG are becoming increasingly important.

A MORO method with different sigma criteria to address the effects of design parametric uncertainties on the optimization design for DFM-CMG is presented in this paper. This paper is organized as follows. The numerical model of DFM-CMG is established by using both 2-D and 3-D FEM and validated by the experiment in Section II. Section III is devoted to the effect of the dimensional parameters of PMs and auxiliary flux modulator (AFM) on ST and STPPC, where the coupling

Manuscript received November 5, 2018; revised November 30, 2018; accepted December 10, 2018. Corresponding author: X. Liu (e-mail: xiaoliu@hnu.edu.cn).

Color versions of one or more of the figures in this paper are available online at http://ieeexplore.ieee.org.

Digital Object Identifier 10.1109/TMAG.2018.2887273

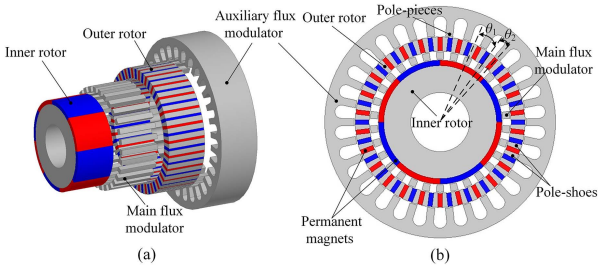

Fig. 1. Topology of DFM-CMG. (a) 3-D exploded view. (b) Front view.

TABLE I
KEY PARAMETERS OF DFM-CMG

Parameter	Value(Unit)
PM thickness of IR (t_{IR})	6 mm
pole-arc coefficient of IR (α_p)	1
PM width of OR (w_{OR})	5 mm
PM length of OR (l_{OR})	15 mm
teeth length of AFM (l_T)	21 mm
yoke length of AFM (l_Y)	12 mm
pole-piece angle of AFM (θ_T)	5 deg
pole-piece angle of MFM (θ_M)	6 deg
air-gap length	1 mm
stack length	60 mm

between the main designparameters of PMs and AFM would be taken into account. Then, the multi-objective particle swarm optimization (MOPSO) algorithm is applied to optimize DFM-CMG using the MORO method based upon the metamodels for improving the torque performance and robustness simultaneously in Section IV. Finally, these conclusions are drawn in Section V.

II. NUMERICAL MODELING OF THE DFM-CMG

A. Finite-Element Modeling

Fig. 1 shows the topology of the studied DFM-CMG. DFM-CMG consists of inner rotor (IR), outer rotor (OR), main flux modulator (MFM), and AFM. The surface-mounted PMs are adopted for IR while spoke-type PMs are employed for OR. The pole pairs of IR and OR are designed as 4 and 26 to form a symmetrical structure helping to eliminate the unbalanced radial magnetic force. IR works as the low-torque input port, and OR is the high-torque output rotor with a gear ratio of 6.5. Like the conventional CMG, stationary MFM is located between IR and OR. The number of pole pieces on MFM is 30, which is the sum of the pole pairs of IR and OR. Specially, a stationary AFM is introduced as the outermost layer to suppress the flux leakages on OR and improve the torque capability. In order to realize the magnetic-gearing effect, the number of pole pieces on AFM has to be equal to the number of pole pieces on MFM. The axis angle between pole piece on AFM and neighboring pole piece on MFM θ_2 is a half of pole-piece pitch angle of MFM θ_1, as shown in Fig. 1. The key design parameters are listed in Table I, and the main geometric parameters of DFM-CMG are shown in Fig. 2.

The FE model of DFM-CMG is developed for calculating the static ST and STPPC on the two rotors by using the 2-D and 3-D Maxwell software. The PM material is NFeB35 with the remanence of 1.23 T, and the density of PMs is 7600 kg/m^3. The yoke of IR and AFM are made of

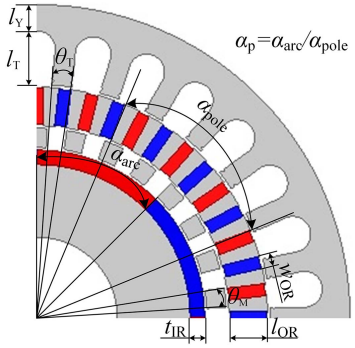

Fig. 2. Main geometric parameters of DFM-CMG.

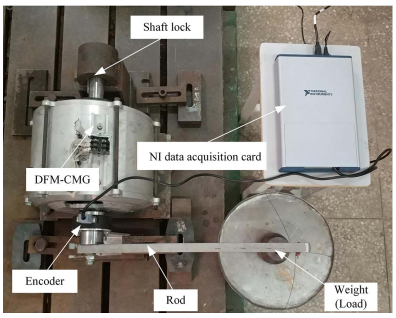

Fig. 3. Test rig for the torque capability of DFM-CMG (top view).

laminated steel sheets DW315_50. Instead of laminated by steel sheets, the pole shoes on OR and pole pieces on MFM are used by a whole piece of 1010 steel. ST on IR and OR calculated by 2-D FEM are 52.6 and 341.9 N·m, respectively. However, the torques of IR and OR calculated by 3-D FEM are only 29.9 and 194.2 N·m, respectively. The corresponding STPPC of DFM-CMG is 117.4 N · m/kg by 2-D FEM and 66.7 N · m/kg by 3-D FEM. The discrepancy is mainly attributed to the considerable end leakage. As there is a huge gap between the 2-D and 3-D FEM simulation results, it is necessary to evaluate the accuracy of FE models before using them for optimization.

B. Validation of the FE Model

In order to validate the FE simulation models, a torsional model of DFM-CMG is established based on two 3-D lookup tables obtained by the 3-D FEM simulation results and mechanical parameters of DFM-CMG. Fig. 3 shows the test rig for the torque capability measurement. OR is locked during the experiment, and an abrupt load torque is applied to IR. Fig. 4 presents the simulation and experimental load angle responses of IR. As could be seen, the end load angle θ and oscillation period obtained from simulation agree well with the experimental results. The tiny discrepancy is probably caused by the compromises made on the manufacture of DFM-CMG.

The oscillation period is defined by the vibration theory

$$T_d = \frac{2\pi}{\sqrt{1-\xi^2}}\sqrt{\frac{J_i}{K}} \quad (1)$$

$$K = P_{in} \times T_{in\_max} \quad (2)$$

where $\delta = \ln(x_t/x_{t+1})$, x_t and x_{t+1} is the amplitude in current cycle and the next cycle, respectively. J_i and K denote the

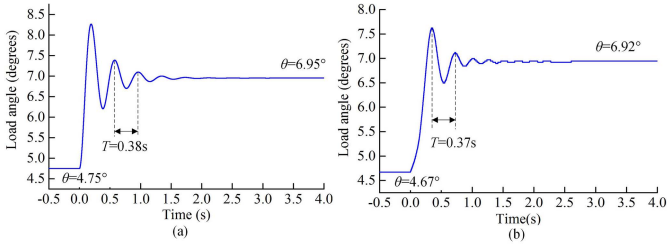

Fig. 4. Load angle oscillation results. (a) Simulation. (b) Experiment.

total moment of inertia and torsional stiffness. The measured value of ST on IR is 29 N · m, which is very close to the 3-D FEM simulation result of 29.9 N · m but far from the 2-D FEM simulation result of 52.6 N · m. As the relative error between the calculated by 3-D FEM and experimental results is 3.10%, the accuracy of the 3-D FE models and simulation results is validated. Therefore, the simulation results of the 3-D FE models are used in Sections III and IV.

III. Parametric Analysis

It has been proven that several dimensional parameters may influence the torque capability of CMGs [7]. The IR PM thickness t_{IR}, the pole-arc coefficient α_{p} of IR, the OR PM width w_{OR} and length l_{OR}, the pole-piece length l_{T} and yoke length l_{Y} of AFM, and the pole-piece angle θ_{T} are selected as the design variables, as shown in Fig. 2. In this section, the impact of aforementioned seven parameters on the torque performance of DFM-CMG is studied, while other unstudied geometric parameters are kept as the initial design.

A. Impact of IR PM Dimensions

The impacts of the IR PM dimensions, i.e., t_{IR} and α_{p}, on the torque performance of DFM-CMG are first analyzed. ST and STPPC of DFM-CMG with different values of t_{IR} and α_{p} while keeping other parameters as constant are shown in Fig. 5. As can be seen from Fig. 5, although a larger t_{IR} and α_{p} may both help to increase ST, t_{IR} plays much more important role than α_{p} in the ST generation. While keeping $t_{\mathrm{IR}} = 6$ mm, ST may grow from 159.2 to 195.0 N · m as α_{p} varies from 0.7 to 1.0. Likewise, ST would increase from 150.7 to 191.9 N · m if t_{IR} changes from 4 to 8 mm, under the condition of $\alpha_{\mathrm{p}} = 0.8$. It is worth noting that the growth rate of ST with increasing t_{IR} and α_{p} would both gradually slow down as shown in Fig. 5(a). As a result, STPPC first increases and then decreases with the increase of t_{IR} and α_{p}. In the case of $t_{\mathrm{IR}} = 6$ mm, STPPC may increase from 61.9 to 67.6 N · m/kg then decrease to 66.9 N · m/kg as α_{p} varies from 0.7 to 1.0.

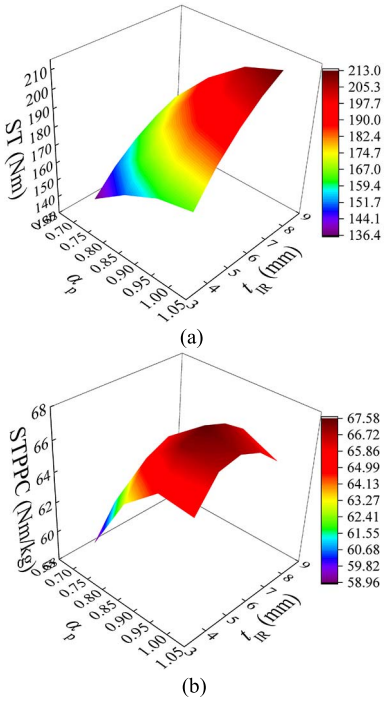

Fig. 5. Variation of the torque performance due to t_{IR} and α_{p}. (a) ST. (b) STPPC.

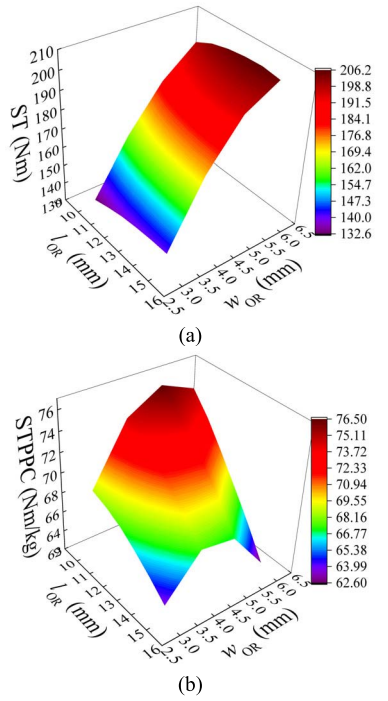

Fig. 6. Variation of the torque performance due to w_{OR} and l_{OR}. (a) ST. (b) STPPC.

B. Impact of OR PM Dimensions

Fig. 6 presents the results of ST and STTPC when w_{OR} and l_{OR} vary within 3–6 and 10–15 mm, respectively. In each case, the other parameters are fixed. As can be seen from Fig. 6, the influence law of w_{OR} and l_{OR} on ST is similar as that shown in Fig. 5(a). It is obvious that the growth rate of ST with the increasing l_{OR} is much slower than that of w_{OR}, indicating that w_{OR} may have bigger impact on ST than l_{OR}. ST would increase from 138.9 to 205.8 N · m if w_{OR} changes from 3 to 6 mm as $l_{\mathrm{OR}} = 13$ mm. However, STPPC would decrease with the increase of l_{OR} due to the significant growth in PM consumption. While keeping $l_{\mathrm{OR}} = 10$ mm, STPPC would achieve the maximum value of 76.5 N · m/kg at $w_{\mathrm{OR}} = 5$ mm.

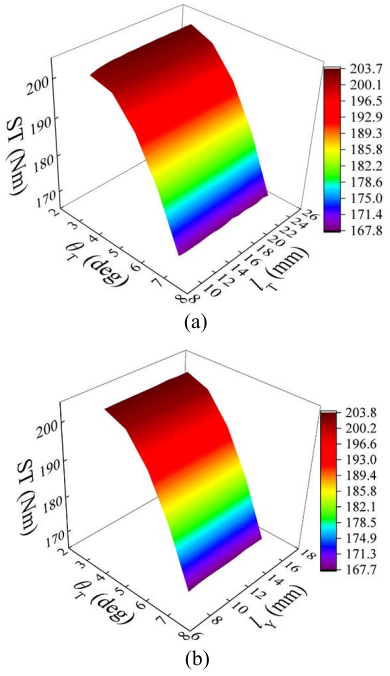

Fig. 7. Variation of ST. (a) Due to l_T and θ_T. (b) Due to l_Y and θ_T.

C. Impact of OR AFM Dimensions

Fig. 7(a) and (b) shows the 3-D curves of ST versus varying l_T and θ_T and l_Y and θ_T, respectively, while keeping other parameters as the initial design. It is clear to see that ST would raise significantly by reducing θ_T, but l_T and l_Y nearly have no effect on ST. ST would be increased from 168.0 to 203.6 N · m if θ_T changes from 7° to 3°. The highest ST could be achieved at $\theta_T = 3°$. Because the parameters of θ_T, l_T, and l_Y do not change the PM consumption, the influence law of these parameters on STPPC would be the same as that shown in Fig. 7.

The aforementioned parametric analysis clearly reveals that ST and STPPC could hardly be affected by l_T and l_Y. However, other five parameters, i.e., t_{IR}, α_p, w_{OR}, l_{OR}, and θ_T, have significant impacts on ST and STPPC of DFM-CMG, which is worth being further optimized.

IV. MORO for the DFM-CMG

A. MORO Model

MODO could not consider the perturbations of design parameters and the reliability and stability of optimization results. In order to take into account of the possible uncertainty in practical dimensions, MORO based on different sigma criteria is employed for optimizing DFM-CMG. In MORO, both the mean value and standard deviation of the design variables and objective functions are considered. The MORO design of DFM-CMG aims to improve the mean value and reduce the variability of ST and STPPC caused by parametric fluctuations, meanwhile, increasing the reliability of design variables and optimization results. Typically, the mathematical model of MORO based on sigma criteria could be expressed as the following equation considering the robustness of both objectives, constraints and design variables, while the two unstudied parameters are kept as the initial design:

$$\begin{cases} \min \quad -\lambda\mu\left[\frac{\mathrm{ST}}{\mathrm{ST_{ref}}}\right]+(1-\lambda)\sigma\left[\frac{\mathrm{ST}}{\mathrm{ST_{ref}}}\right] \\ \qquad -\lambda\mu\left[\frac{\mathrm{STPPC}}{\mathrm{STPPC_{ref}}}\right]+(1-\lambda)\sigma\left[\frac{\mathrm{STPPC}}{\mathrm{STPPC_{ref}}}\right] \\ \text{s.t. } 4\ \mathrm{mm}+n\sigma[t_{IR}] \le \mu[t_{IR}] \le 8\ \mathrm{mm}-n\sigma[t_{IR}] \\ \quad 0.7+n\sigma[a_p] \le \mu[a_p] \le 1.0-n\sigma[a_p] \\ \quad 3\ \mathrm{mm}+n\sigma[w_{OR}] \le \mu[w_{OR}] \le 6\ \mathrm{mm}-n\sigma[w_{OR}] \\ \quad 10\ \mathrm{mm}+n\sigma[l_{OR}] \le \mu[l_{OR}] \le 15\ \mathrm{mm}-n\sigma[l_{OR}] \\ \quad 3\ \mathrm{deg}+n\sigma[\theta_T] \le \mu[\theta_T] \le 7\ \mathrm{deg}-n\sigma[\theta_T] \end{cases} \tag{3}$$

where μ and σ are the mean and standard deviation, respectively, and λ denotes the weight factors imposed on the mean of the optimization results. $\mathrm{ST_{ref}}$ and $\mathrm{STPPC_{ref}}$, which are introduced to make two objectives comparable, are the reference value of ST and STPPC with the initial design, respectively. In (3), the value of n is typically set as 3 or 6, namely, three sigma (3σ) or six sigma (6σ), which is used to control the width of the distribution. In this paper, each design parameter is assumed to distribute normally with the standard deviation as 1/3 (3σ) or 1/6 (6σ) of its manufacturing tolerance. The tolerance values of each design parameter are equal to 5% of their variation range from the typical manufacturing tolerance. Besides, the sigma criteria of objectives and design variables are set as the same.

A typical method to generate sample points is to adopt the design of experiments. The full factorial design method, noted for its uniformity, is implemented to generate 2400 sample points. Based on the sample points obtained by 3-D FEM of DFM-CMG, the metamodels based on PR are established to approximate the functions of ST and STPPC with the five main design parameters, which are expressed as

$$\begin{aligned} \mathrm{ST} = {} & -400.24+17.55\theta_T+12.28l_{OR}+12.39t_{IR} \\ & +47.40w_{OR}+453.03a_p-1.64\theta_T^2-0.43l_{OR}^2 \\ & -1.25t_{IR}^2-4.04w_{OR}^2-248.77a_p^2+0.01\theta_T l_{OR} \\ & -0.60\theta_T t_{IR}-0.91\theta_T w_{OR}-3.42\theta_T a_p \\ & -0.01l_{OR}t_{IR}-0.07l_{OR}w_{out}+0.06l_{OR}a_p \\ & +1.42t_{IR}w_{OR}+10.20t_{IR}a_p+7.67w_{OR}a_p \end{aligned} \tag{4}$$

$$\begin{aligned} \mathrm{STPPC} = {} & -44.11+0.82\theta_T+0.15l_{OR}+0.80t_{IR} \\ & +17.60w_{OR}+201.43a_p-0.70\theta_T^2-0.11l_{OR}^2 \\ & -0.45t_{IR}^2-1.78w_{OR}^2-114.19a_p^2+0.18\theta_T l_{OR} \\ & -0.01\theta_T t_{IR}+0.05\theta_T w_{OR}+0.30\theta_T a_p \\ & +0.21l_{OR}t_{IR}-0.47l_{OR}w_{out}+0.79l_{OR}a_p \\ & +0.64t_{IR}w_{OR}-1.55t_{IR}a_p+1.07w_{OR}a_p. \end{aligned} \tag{5}$$

The accuracies of these metamodels can be evaluated by the root-mean-square error normalized (RMSEN), the maximum error normalized (MEN), and the square value (R^2), which can be given by

$$\mathrm{RMSEN} = \frac{\sqrt{\frac{\sum_{k=1}^{n}(y_k-\hat{y}_k)^2}{n}}}{y_{k\_\max}-y_{k\_\min}} \tag{6}$$

$$\mathrm{MEN} = \left(\frac{\max|y_k-\hat{y}_k|}{y_{k\_\max}-y_{k\_\min}}\right), \quad k=1,2,\ldots,n \tag{7}$$

TABLE II
ACCURACY ASSESSMENT OF THE METAMODELS

	RMSEN	MEN	R^2
ST	0.0155	0.0294	0.9965
STPPC	0.0166	0.0323	0.9963

$$R^2 = 1 - \frac{\sum_{k=1}^{n} (y_k - \hat{y}_k)^2}{\sum_{k=1}^{n} (y_k - \bar{y}_k)^2} \tag{8}$$

where y_k and $\hat{y}_k$ represent the exact response value calculated by FEM and the corresponding value predicted by PR metamodels for the error analysis point k, $\bar{y}_k$ is the average of y_k, and n denotes the number of these error analysis sample points. It is worth noting that smaller RMSEN and MEN are preferred, and the value of R^2 closer to 1 indicates a higher accuracy for the overall design space. The results of accuracy assessments of these PR metamodels are listed in Table II. It could be seen that R^2 for ST and STPPC metamodels are 0.9965 and 0.9963, both very close to 1. It proves that these responses of ST and STPPC can be predicted by the PR metamodels accurately. Therefore, these metamodels would be employed in the following MODO and MORO with reliable accuracy.

In order to illustrate the performance of different sigma criterion, the reliability of all design variables P_{var} is taken as a criterion according to the multiplication theorem of independent events in statistics, which is defined as

$$P_{\text{var}}(X_i) = \prod_{i=1,2,\ldots,m} P(\text{LL}_i \le X_i \le \text{UL}_i) \tag{9}$$

where m denotes the number of design variables, P is the reliability of each design variable, and the LL and UL are the lower and upper limits of design variables.

B. MORO Method

Fig. 8 shows the flowchart of the developed MORO design method. Compared with other multi-objective optimization algorithms such as NSGA-II, the MOPSO algorithm is characterized by fast convergence and well-distributed Pareto frontier [13]. Moreover, it is worth noting that the MOPSO algorithm has been employed to solve the design problems of electromagnetic devices with PM successfully [14].

In this method, the metamodels of ST and STPPC based upon the full factorial design method and the PR technique are constructed. The MOPSO algorithm is first employed to maximize ST and STPPC in MODO. In order to compute the probability distribution of design variables and objective functions, it is assumed that the design variables are independent and normally distributed. The reliability of design parameters from MODO is evaluated according to (9). The lowest reliability is set to 95.0%, if the reliability of design parameters is lower than 95.0%, the MOPSO algorithm-based MCS would be used to handle with the MORO design to increase the robustness of the optimal designs and prevent the limit violation. For each of the design variables and objective functions in MORO, 10 000 MCSs are employed to get the statistic characteristics.

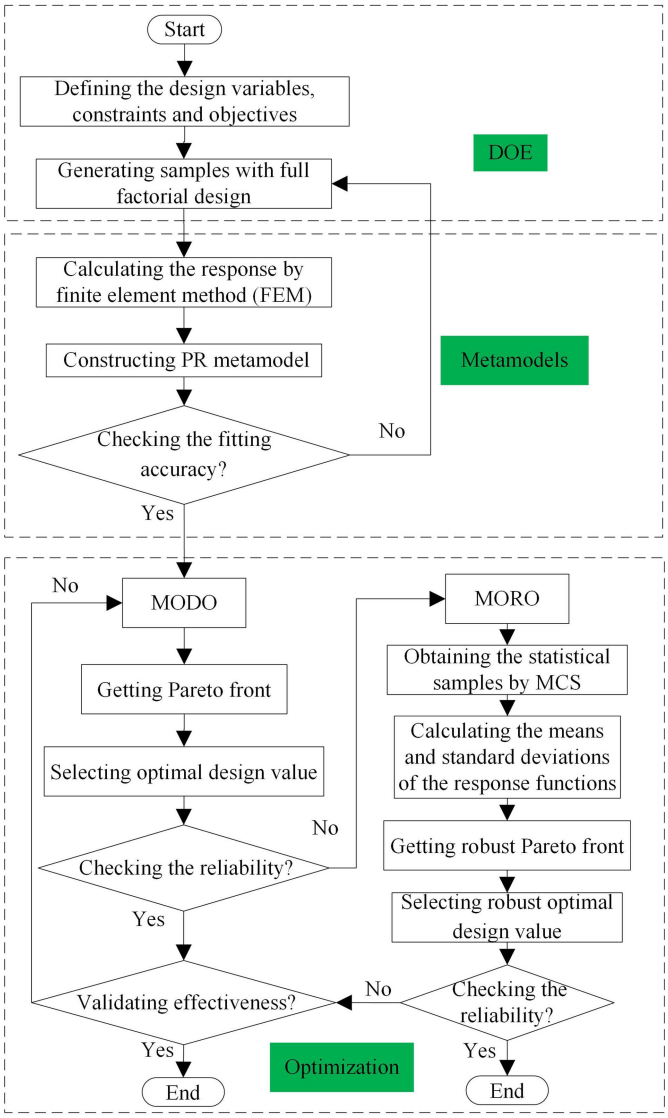

Fig. 8. Flowchart of MORO.

C. Optimization Results and Discussion

The MOPSO algorithm is first employed to solve the MODO problem without considering the perturbations and uncertainty of design variables. The settings of MOPSO are listed in Table III. The Pareto frontier for DFM-CMG converges adequately after 1000 generations. Every point on the Pareto fronts represents one Pareto optimal solution, which elucidates the tradeoff between ST and STPPC. It is also found that an optimal design as point D shown has a higher STPPC with a 22.5% growth when maintaining ST to be compared with the initial design point I. Moreover, the optima at right side of point D, in the green-dotted area as shown in Fig. 9, could increase ST and STPPC simultaneously compared with the initial design. The highest ST is achieved at 238.0 N·m by only taking torque capability into account, while the highest STPPC could be improved to 82.3 N·m/kg by 3-D FEM. The design parameters and their reliability of MODO are given in the second and third columns of Table IV. The reliability

TABLE III
SETTINGS OF MOPSO

MOPSO setting parameter	Value
Population size	100
External archive size	50
Inertial weight	0.730
Personal learning coefficient	1.496
Global learning coefficient	1.496

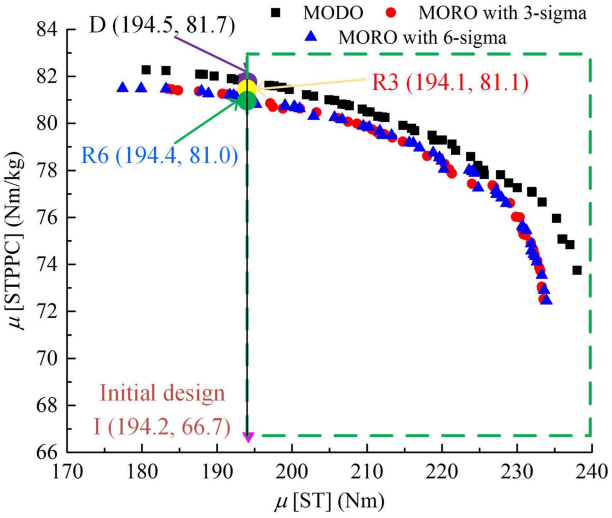

Fig. 9. Pareto fronts of mean value with MODO and MORO ($\lambda = 1$).

TABLE IV
DESIGN PARAMETERS AND OPTIMIZATION RESULTS

Design parameter	MODO	P	MORO 3-σ	P	MORO 6-σ	P
t_{IR}	6.13 mm	100.0%	6.02 mm	100.0%	6.25 mm	100.0%
α_p	0.92	100.0%	0.92	100.0%	0.92	100.0%
w_{OR}	5.20 mm	100.0%	5.22 mm	100.0%	5.11 mm	100.0%
l_{OR}	10.00 mm	50.2%	10.25 mm	99.9%	10.25 mm	100.0%
θ_T	3.06 deg	80.6%	3.20 deg	99.9%	3.20 deg	100.0%

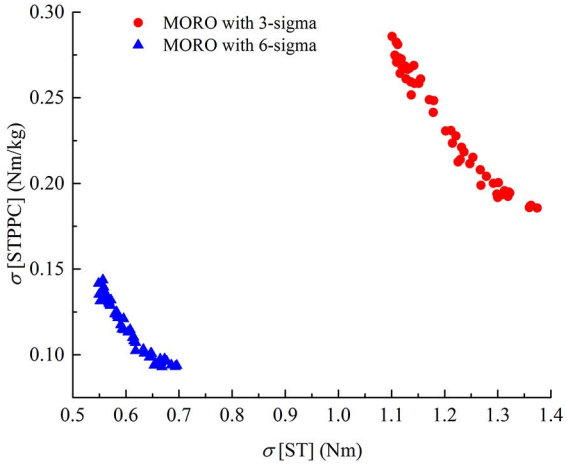

Fig. 10. Pareto fronts of standard deviation for MORO with 3σ and 6σ ($\lambda = 1$).

calculated according to (9) is 40.5%, which means that the reliability of the optimal results is lower than the acceptable value.

In order to increase the stability of the optimal designs and improve the reliability of design parameters, it is necessary to implement MORO for the DFM-CMG design. The Pareto fronts are obtained for 3σ and 6σ with $\lambda = 1$ using the MORO method described in Fig. 8. The comparisons of Pareto fronts of MODO ($n = 0$) and MORO are shown in Fig. 9. The Pareto fronts of MORO all locate to the lower left of the MODO points, indicating that MORO has a lower probability to violate constraint near the range boundary of the design parameters caused by the parameter variation. In addition, it is also found that the shape of the Pareto fronts is similar to the 3σ and 6σ criteria. The design parameters of MODO and MORO with 3σ and 6σ are given in Table IV. The reliabilities of MODO and MORO with 3σ and 6σ are 40.5%, 99.8%, and 100.0%, respectively, which means that the reliability of the optimal results with MORO is significantly improved.

Fig. 10 shows the optimal Pareto fronts of the standard deviation for MORO with 3σ and 6σ. It could be seen that the standard deviations with 6σ is much lower than these with 3σ, indicating that the Pareto fronts with 6σ becomes more reliable.

The comparisons between the optimal results of MODO and MORO are listed in Table V. STPPC achieved by MORO with 6σ is a little lower than that of MODO, which has a 21.4% and 22.5% growth than that of the initial design under the same constraint of ST, respectively. However, the standard

TABLE V
ERROR OF OPTIMIZATION METHOD

		μ[ST]	μ[STPPC]	σ[ST]	σ[STPPC]
MODO	Metamodel	194.53 Nm	81.71 Nm/kg	1.32 Nm	0.18 Nm/kg
	FEM (3D)	194.42 Nm	81.68 Nm/kg	1.31 Nm	0.18 Nm/kg
	Error	0.06%	0.04%	0.06%	0.05%
MORO 3-σ	Metamodel	194.11 Nm	81.11 Nm/kg	1.31 Nm	0.19 Nm/kg
	FEM (3D)	194.01 Nm	81.08 Nm/kg	1.30 Nm	0.19 Nm/kg
	Error	0.05%	0.04%	0.08%	0.06%
MORO 6-σ	Metamodel	194.42 Nm	81.01 Nm/kg	0.66 Nm	0.10 Nm/kg
	FEM (3D)	194.32 Nm	80.98 Nm/kg	0.65 Nm	0.10 Nm/kg
	Error	0.05%	0.04%	0.15%	0.07%

deviations of ST and STPPC are 0.66 N · m and 0.10 N · m/kg which are much lower than those of 1.32 N·m and 0.18 N·m/kg obtained by MODO. It proves that the stability of MORO results is higher than that of the MODO results. Moreover, it could be found that these errors of ST and STPPC between the FEM results and the optimization results based on the metamodels are less than 0.2% from Table V, which demonstrates the effectiveness of the MODO and MORO methods. In addition, a higher robustness could be expected with higher sigma criteria considering the perturbations and uncertainty of the design variables. However, the mean values may be decreased at the same time. For industrial manufacturing and assembling, 3σ criteria mean 2700 defects per million for the short term and 66 803 defects per million for the long term, while 6σ criteria signify 0.002 defects per million for the short term, and 3.4 defects per million for the long term [15]. In order to enhance the robustness of the optimization

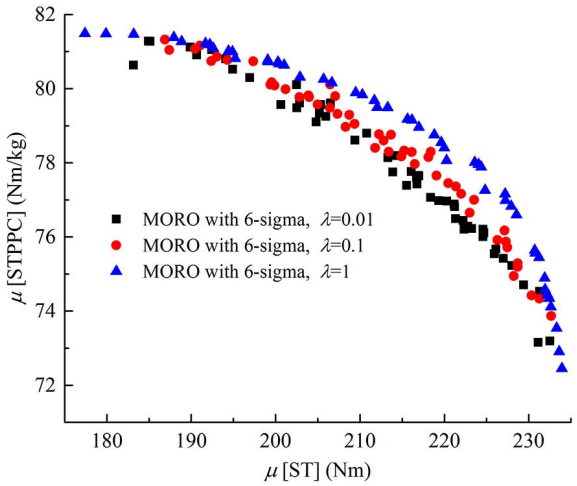

Fig. 11. Pareto fronts of mean value for MORO with 6σ.

results effectively, MORO designed for DFM-CMG is expected to achieve 6σ criteria in this paper.

Fig. 11 presents the optimal Pareto fronts using MORO-based 6σ criterion with $\lambda = 1$, $\lambda = 0.1$, and $\lambda = 0.01$, respectively. The ranges and shapes of the Pareto fronts are similar to that shown in Fig. 9. It is worth noting that the Pareto fronts moves to the lower left as the decrease of λ, indicating that the mean values of ST and STPPC are worse when the weight factors λ imposed on the standard deviation of the optimization results is considered.

Although large number of optimization points could be gotten from the Pareto frontiers, the most satisfactory optimization results should be chose from the Pareto frontiers finally. Usually, the weight method is used, in which transforming many objectives into a single objective function based on weight factors in according to their relative significance. However, it is not easy to set suitable weight factors imposed on each objective. The minimum distance selection method presented in [16] is used to obtain the most optimal design point from Pareto frontiers. In this paper, the schematic of the minimum distance selection method considering the normalized objective functions is shown in Fig. 12. f_1 and f_2 are the normalized values of both objective functions on the Pareto front. The point (1, 1) denotes the ideal optimal solution that is unachievable due to the confliction of two different objectives. The variable distance D represents the distance from optimization points on the Pareto front to the ideal point. The most satisfactory solution termed as the overall optimum point has the shortest distance $D_{\min}$ shown in Fig. 12.

The most satisfactory solution points for the Pareto frontiers shown in Fig. 11 are obtained by adopting the aforementioned method. In this case, f_1 and f_2 are defined as the mean values of ST and STPPC, respectively. The comparative results are summarized in Table VI. It could be found that these overall optimum points centrally distribute in lower right region under different values of λ. Moreover, the smaller λ, the lower mean values, and standard deviations of ST and STPPC for the optimization results are obtained. Therefore, the tradeoff must be made between the stability and the torque performance in practice.

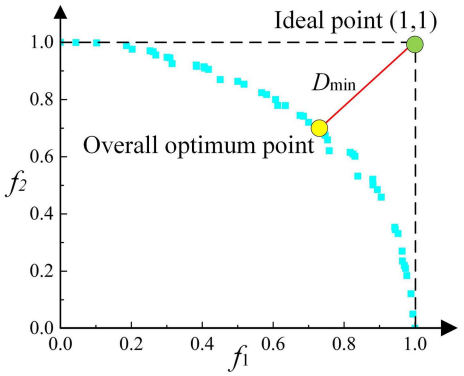

Fig. 12. Schematic of the shortest distance selection method based on normalized objective functions.

TABLE VI
COMPARISON OF OPTIMIZATION RESULTS

	μ[ST]	μ[STPPC]	σ[ST]	σ[STPPC]
$\lambda = 1$	218.81 Nm	78.75 Nm/kg	0.60 Nm	0.12 Nm/kg
$\lambda = 0.1$	218.38 Nm	78.30 Nm/kg	0.59 Nm	0.11 Nm/kg
$\lambda = 0.01$	214.21 Nm	78.20 Nm/kg	0.58 Nm	0.10 Nm/kg

V. CONCLUSION

In order to improve the torque performance and robustness of DFM-CMG simultaneously during the design process, a MORO method addressing the effects of parametric uncertainties on the optimization design is presented in this paper. The MOPSO algorithm with MCS is employed to conduct MORO. The optimized results show that STPPC achieved by MORO with 6σ has a 21.4% growth than that of the initial design under the same constraint of ST. Compared with the MODO results, although the optimized STPPC of MORO with 6σ result decreases by 1.1%, the robustness could be significantly improved. It is proven that the MORO design method is effective to achieve higher stability and reliability as well as the torque performance of DFM-CMG, which could help to improve the comprehensive performance of the novel DFM-CMG in practical applications.

ACKNOWLEDGMENT

This work was supported by the National Natural Science Foundation of China under Grant 51877074.

REFERENCES

[1] T. B. Martin, Jr., "Magnetic transmission," U.S. Patent 3 378 710 A, Apr. 16, 1968.
[2] K. Atallah and D. Howe, "A novel high-performance magnetic gear," *IEEE Trans. Magn.*, vol. 37, no. 4, pp. 2844–2846, Jul. 2001.
[3] X. Zhang, X. Liu, and Z. Chen, "A novel dual-flux-modulator coaxial magnetic gear for high torque capability," *IEEE Trans. Energy Convers.*, vol. 33, no. 2, pp. 682–691, Jun. 2018.
[4] S.-J. Kim, C.-H. Kim, S.-Y. Jung, and Y.-J. Kim, "Shape optimization of a hybrid magnetic torque converter using the multiple linear regression analysis," *IEEE Trans. Magn.*, vol. 52, no. 3, Mar. 2016, Art. no. 8102504.
[5] Q. Wang, S. Niu, and S. Yang, "Design optimization and comparative study of novel magnetic-geared permanent magnet machines," *IEEE Trans. Magn.*, vol. 53, no. 6, Jun. 2017, Art. no. 8104204.
[6] Y. C. Wang, S. Niu, and W. Fu, "Sensitivity analysis and optimal design of a dual mechanical port bidirectional flux-modulated machine," *IEEE Trans. Ind. Electron.*, vol. 65, no. 1, pp. 211–220, Jan. 2018.

[7] M. Filippini and P. Alotto, "Coaxial magnetic gear design and optimization," *IEEE Trans. Ind. Electron.*, vol. 64, no. 12, pp. 9934–9942, Dec. 2017.

[8] B. Ma, G. Lei, J. Zhu, Y. Guo, and C. Liu, "Application-oriented robust design optimization method for batch production of permanent-magnet motors," *IEEE Trans. Ind. Electron.*, vol. 65, no. 2, pp. 1728–1739, Feb. 2018.

[9] M. Johnson, M. C. Gardner, H. A. Toliyat, S. Englebretson, W. Ouyang, and C. Tschida, "Design, construction, and analysis of a large-scale inner stator radial flux magnetically geared generator for wave energy conversion," *IEEE Trans. Ind. Appl.*, vol. 54, no. 4, pp. 3305–3314, Jul./Aug. 2018.

[10] X. Meng *et al.*, "Robust multilevel optimization of PMSM using design for six sigma," *IEEE Trans. Magn.*, vol. 47, no. 10, pp. 3248–3251, Oct. 2011.

[11] G. Lei, J. G. Zhu, Y. G. Guo, J. F. Hu, W. Xu, and K. R. Shao, "Robust design optimization of PM-SMC motors for six sigma quality manufacturing," *IEEE Trans. Magn.*, vol. 49, no. 7, pp. 3953–3956, Jul. 2013.

[12] M. Chen, K. T. Chau, W. Li, and C. Liu, "Cost-effectiveness comparison of coaxial magnetic gears with different magnet materials," *IEEE Trans. Magn.*, vol. 50, no. 2, pp. 821–824, Feb. 2014.

[13] C. A. C. Coello, G. T. Pulido, and M. S. Lechuga, "Handling multiple objectives with particle swarm optimization," *IEEE Trans. Evol. Comput.*, vol. 8, no. 3, pp. 256–279, Jun. 2004.

[14] X. Ye, H. Chen, H. Liang, X. Chen, and J. You, "Multi-objective optimization design for electromagnetic devices with permanent magnet based on approximation model and distributed cooperative particle swarm optimization algorithm," *IEEE Trans. Magn.*, vol. 54, no. 3, Mar. 2018, Art. no. 8000604.

[15] B. Ma, G. Lei, C. Liu, J. Zhu, and Y. Guo, "Robust tolerance design optimization of a PM claw pole motor with soft magnetic composite cores," *IEEE Trans. Magn.*, vol. 54, no. 3, Mar. 2018, Art. no. 8102404.

[16] D. Zhang, Z. Ren, and C.-S. Koh, "Optimal design of powder-aligning and magnetizing fixtures for an anisotropic-bonded NdFeB permanent magnet," *IEEE Trans. Magn.*, vol. 50, no. 2, Feb. 2014, Art. no. 7017204.